Programmable Kerr Combs in Laser Cavity Soliton Mode-Locked Laser

ALEXIS BOUGAUD,[1,*] MANAL ARBATI,[1] BRUNO P. CHAVES,[1] THOMAS BUNEL,[2] ANTONIO CUTRONA,[3] ARNAUD MUSSOT,[2] ALESSIA PASQUAZI,[3] BENJAMIN WETZEL[1,†]

[1] *Xlim Research Institute, CNRS UMR 7252, Université de Limoges, 87060, Limoges, France*
[2] *Université de Lille, CNRS UMR 8523—PhLAM—Physique des Lasers Atomes et Molécules, F-59000, Lille, France*
[3] *Emmergent Photonics Research Centre, Dept. of Physics, Loughborough University, Loughborough, LE11 3TU, England, UK*
*alexis.bougaud@xlim.fr ; †benjamin.wetzel@xlim.fr

Received XX Month XXXX; revised XX Month, XXXX; accepted XX Month XXXX; posted XX Month XXXX (Doc. ID XXXXX); published XX Month XXXX

We numerically study programmable Kerr comb mode-locked fiber laser based on a nested cavities architecture. The nested architecture includes an optical resonator as well as a photonic device used as programmable delay-line, which allows for controlling the pulse repetition rate of a passively mode-locked laser over a frequency range covering the GHz-THz interval. In the proposed approach, the pulse repetition rate is adjusted based on a temporal interleaving process, obtained after propagation through the programmable delay-line structure. Our numerical study demonstrates how a programmable delay-line can be leveraged to obtain a highly-tunable Kerr-comb laser via harmonic mode-locking, featuring the formation of energy efficient yet reconfigurable laser cavity soliton pulses. In particular, basic rules are outlined to facilitate the experimental implementation of such a mode-locked laser. The proposed laser architecture is expected to thus provide enhanced versatility for compact and tunable frequency comb generation.

Broadband and stable optical frequency comb (OFC) are commonly generated nowadays by mode-locked lasers, allowing for the emission sub-picosecond pulses with mature stabilization technics [1]. Passive mode-locked strategies based on saturable absorber [2], pulse colliding mode-locking [3] and more recently, microcavities [4] appeared to be particularly efficient regarding the OFC spectral bandwidth and pulse repetition rate. Nevertheless, all those solutions suffer from a lack of tunability, so that different Mode Locked-Laser (MLL) cavities has to be designed for specific applications such as dual-comb ranging [5] or direct comb-based spectroscopy [6]. At the same time, the recent development of photonic integrated circuits (PICs) allows an accurate control of the optical path down to the nanometer scale [7]. This accuracy became highly valuable for the control of coherent process such as interferometric pattern obtained by e.g. Mach-Zehnder Interferometer (MZI) structures. Such integrated approaches already demonstrated strong potential for pulse reshaping [8] and with direct applications for nonlinear fiber dynamics control [9] to quantum signal processing [10]. In this paper, we leverage this architecture and present a passive fiber MLL based on a nested cavity configuration for Kerr comb generation, including a PIC used as Programmable Delay Line (PDL) [11] which allow a passive repetition rate multiplication by pulse interleaving operation. The proposed laser architecture is expected to circumvent the lack of tunability for pulse repetition rate within passive mode-locking OFC architectures.

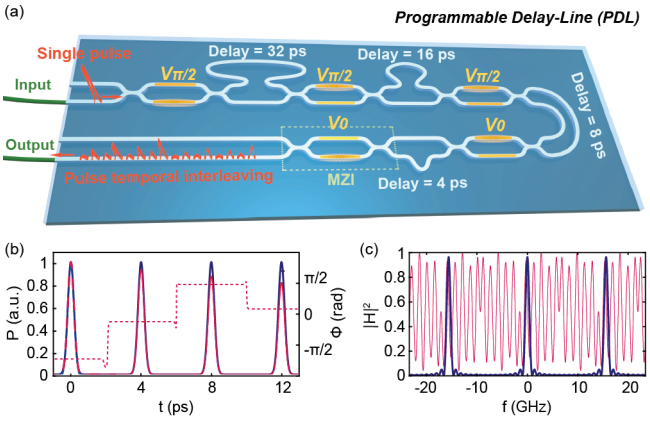

Fig. 1. (a) Artistical view of a PDL with a unitary delay $\tau_0 = 1\ ps$. Each delay-line are coupled by two MZI used as power splitter. The sequence of voltages displayed allow the pulse splitting presented on (b). (b) Pulse splitting operation of an initial 400 fs pulse width (dashed red) into a train of separated pulse with (red) and without (dark) delay-line losses. The phase steps induced by the MZI are also shown (dotted red). (c) Transfer function of an ideal pulse interleaving $|H_{ideal}|^2$ (blue) and the PDL transfer function $|H_{PDL}|^2$(red) for l=4 (i.e. $T_{rep} = T_0/2^4$ in eq. (3)).

The PDL is a PIC formed by two optical paths of different length (Fig.1a). The shorter is used as reference and the longer as a delay-line. Those two paths are locally coupled by a set of March Zehnder Interferometer (MZI), and divided into a subset of delay-lines, the nth delay-line being related to the next one by the relationship: $\tau_{n+1} = \tau_n/2$. The MZI are used

as a variable coupler to control the optical path followed by each optical pulse oscillating in the laser cavity. When used with a coupling ratio of 50:50, the PDL interleaves the pulse train temporally and, eventually, multiples the pulse repetition rate whenever the delay provided by the PDL relationship commensurable with the laser cavity period, so that: $\tau_{PDL} = T_0/2^n$ (with T_0 being the fundamental period of the MLL and with $n \in \mathbb{N}$). In this regime, adjustable harmonic oscillations become accessible for passive MLL. This approach allows combining the repetition rate tunability usually obtained by active MLL with the broadband spectrum typically featured by passive MLL. In fact, the repetition rate control offered by the PDL becomes particularly valuable when included in a Kerr comb MLL within a nested cavities configuration. For such a structure, the fundamental repetition rate can be chosen with the length of the high Q-factor resonator, while its harmonics are obtained by making the length of the PDL delay lines in the external cavity commensurable with the resonator one. For a resonator length on the order of cm, this structure can be considered as a solution able to bridge the gap between the radiofrequency and the terahertz range (GHz-THz), and thus can have numerous applications for wireless systems (6G) and telecommunications beyond the current standard 4G/IMT [12].

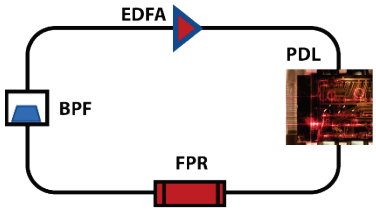

Fig.2. Scheme of the (realistic) nested cavity setup considered in simulations: BPF: band-pass filter, EDFA: Erbium Doped Fiber Amplifier, FPR: Fabry-Pérot Resonator, PDL: Programmable Delay-Line.

The MLL proposed in Fig. 2 is built upon a main fiber cavity of 20.88 m, yielding a global Free Spectral Range (FSR) of 9.76 MHz and encompassing an EDFA, a band-pass filter (centered at 1560 nm with 2 nm linewidth), a PDL, and a Fabry-Perot fiber resonator (FPR) [13]. The FPR, used as auxiliary cavity, presents an FSR of 976 MHz, with a Full Width at Half Maximum (FWHM) linewidth of 5 MHz. The fundamental period of the Kerr-comb laser is thus $T_0 = 1024$ ps, and other cavity parameters are summarized on the supplementary Table.S1, in physical units. The system is modeled following a mean field method, with the standard normalization of the Lugiato-Lefever equation [14]. As a result, we obtain the system of coupled equations (1), including the impulse response $h_{PDL}(\phi)$ of the PDL (where $*$ stands for convolution product, ψ_a and ψ_b respectively the normalized FPR intra-cavity and fiber ring loop fields):

$$\begin{aligned}\frac{\partial\psi_a}{\partial t} &= \left[-\frac{\kappa_a}{\kappa_b} - id_{2a}\frac{\partial^2}{\partial\phi^2} + d_{3a}\frac{\partial^3}{\partial\phi^3} + i\right.\\ &\left.\left(|\psi_a|^2 + \frac{2}{\phi_0}\int|\psi_a|^2 d\phi\right)\right]\psi_a + k_{b\to a}\psi_b\\ \frac{\partial\psi_b}{\partial t} &= \left[-\left(1 + \frac{2}{\kappa_b.T_b} + i\delta_0\right) - \zeta_b\frac{\partial}{\partial\phi} - \frac{i}{2}(2d_{2b} - i\sigma_b)\frac{\partial^2}{\partial\phi^2} + \right.\\ &\left. d_{3b}\frac{\partial^3}{\partial\phi^3} + \frac{g_{0,EDFA}}{1+\left|\frac{\psi_b}{\psi_{b,sat}}\right|^2}\right]\psi_b + h_{PDL}(\phi) * \psi_b + k_{a\to b}\psi_a\end{aligned} \quad (1)$$

The PDL can be modeled as a sequence of transfer functions. Each MZI, used as variable couplers, can then be modeled as follow:

$$T_{MZI}(V_n) = M_c M(V_n) M_c$$

$$M_c = \begin{bmatrix}\sqrt{1-\alpha} & i\sqrt{\alpha}\\ i\sqrt{\alpha} & \sqrt{1-\alpha}\end{bmatrix}$$

$$M(V_n) = \begin{bmatrix}1 & 0\\ 0 & \exp\left(i\pi\frac{V_n}{V_\pi}\right)\end{bmatrix}$$

$$M_n(i\omega) = \begin{bmatrix}1 & 0\\ 0 & \exp(-l_n + i(\beta_{\Sigma\,0,PDL\,n} + \beta_{\Sigma\,1,PDL\,n}\omega))\end{bmatrix}$$

M_c is the transfer matrix for a coupler with α as coupling ratio. $M(V_n)$ includes the phase difference induced by applying a voltage V_n onto the nth MZI, which can be used to adjust the power splitting ratio between the two arms of the PDL. V_π represents the particular voltage for which the two arms of the PDL switch their respective optical power. Finally, $M_n(i\omega)$ considers the propagation of each individual delay-line in the PDL (ω being the angular frequency centered around the optical carrier). The first row represents the propagation in the short arm of the PDL, while the second row represents the propagation in the long arm (i.e. the delay-line). Here, we only consider the additional loss (l_n) and the phase difference between the two arms ($\beta_{\Sigma\,0,PDL\,n}$ being the carrier phase shift the nth delay-line and $\beta_{\Sigma\,1,PDL\,n}$ its corresponding delay), so that the transfer function of the short arm is represented by the identity. Considering a succession of $N = 8$ delay-lines, the global PDL transfer function associated with a set of N+1 voltages $\{V_n\}_{1\le n\le N+1}$ to control the optical path along the PDL can then be written as:

$$H_{PDL}(i\omega) = T_{MZI}(V_{N+1})\prod_{n=1}^{N} M_n(i\omega).T_{MZI}(V_n) \quad (2)$$

This transfer function is injected into the mean field equation system (1). For simplicity, we here only consider two voltage values: V_0 for a fully transmitted signal and $V_{\pi/2}$ for a 50:50 splitting ratio between the two arms. As a result, a pulse interleaving operation results in a succession of $V_{\pi/2}$ sequence (for pulse splitting and delay operation), each of them leading to a decimation of the pulse period by a factor 2, followed by a set of V_0 once the required pulse period is reached (Fig.1a). Noteworthy, each $V_{\pi/2}$ splitting operation induces a $\pi/2$ phase step on the optical carrier and leads to major discrepancies on the PDL transfer function $T_{PDL}(i\omega)$ compared to a pure delay operation. Considering a pulse

interleaving operation based on a pure delay, the PDL transfer function can be written as:

$$H_{ideal}(i\omega) = 2\exp\left(\frac{i}{2}\left(1-\frac{1}{2^l}\right)T_0\omega\right).\left(\sum_{p=0}^{2^{l-2}}\cos\left((2p+1)\frac{T_0\omega}{2^{l+1}}\right)\right) \quad (3)$$

so that the pulse repetition rate at the end of the PDL is divided by 2^l ($T_{rep} = T_0/2^l$). In such an ideal case, the PDL acts has a *sinc*-like filter in the spectral domain (red line in Fig.1c), thus providing a clear modal selection enabling MLL harmonic operation. Yet, in a realistic case, the phase step imposed by the MZI splitter (see Fig.1b) significantly deteriorate the PDL modal selectivity, yielding more restrictive locking conditions to achieve stable lasing operation. However, while the PDL phase step alter the global mode-locking dynamics, we had no difficulties to numerically obtain a steady-state by merely adjusting the cavity gain and the detuning between the two cavities following the bifurcation diagram of laser cavity soliton theory [4]. This shows that despite the apparent complexity of the PDL transfer function, the stability of the MLL and its capacity to readily emit laser cavity soliton remain close to a standard nested cavity architecture.

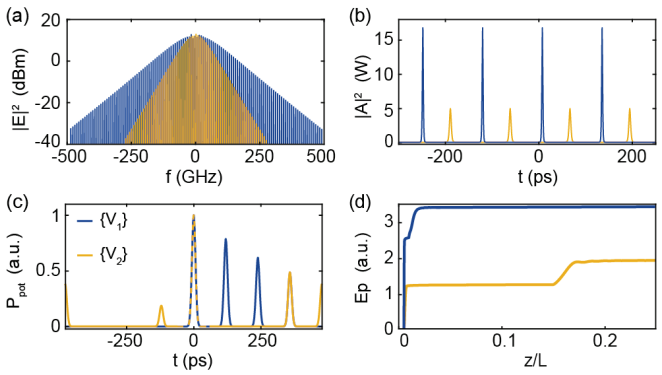

Fig. 3. (a) Optical spectrum and (b) temporal intensity of two steady-states achieved within the programmable MLL. The two steady-states were achieved based on different sets of PDL voltages: $\{V_1\}$ (blue), $\{V_2\}$ (yellow), respectively. (c) PDL pulse splitting obtained for $\{V_1\}$ and $\{V_2\}$, and leading to an identical minimal delay (τ) between successive pulses. (d) Evolution of the auxiliary intra-cavity energy with the distance of propagation, leading to the steady-state shown on (a-b).

Recalling that pulse interleaving allows to multiply the pulse repetition rate at each round trip (Fig.1b) and act as an optical filter (Fig.1c), whether the delay-line losses are neglected, we note that identical pulse repetition rate can be obtained from different PDL configurations when considering a rational mode-locking approach. In this case, pulse interleaving is achieved after 2^n round trips instead of a single one. To illustrate this rational mode-locking behavior, we consider the simple case of a pulse divided into two delayed replicas by the nth PDL interferometer, so that the delay between the two pulses is $\tau = T_0/2^n$. In this case, pulse splitting needs to be repeated 2^n times to meet the fundamental period of the MLL and reach harmonic oscillation. The phase condition for the oscillation is achieved after 2^n cavity round trip, just as the gain condition, recalling standard rational mode-locking condition for MLL. In our realistic PDL structure [9], each unit delay is related to the next by $\tau_{n+1} = \tau_n/2$, so that the steady-state repetition rate will be fixed by the minimal delay imposed by the PDL interleaving operation (Fig.3c). Now, considering the propagation losses induced by each delay-line, the pulse interleaving operation always split each pulse into a sub-pulse train of decreasing amplitude. As a result, the actual mode-locking including the PDL is always achieved after 2^n round trips. The choice of the PDL settings will then only impact the spread of the optical power over the fundamental period of the MLL at each round trip, and thus the gain condition required to achieve rational mode-locking.

Numerical simulations show that the locking bandwidth (i.e. the detuning between the main and auxiliary cavities) increases along with the number of pulse splitting operated by the PDL (i.e. as the optical power is spread over the fundamental period). The gain required to achieve stable oscillation is also reduced. For instance, Fig.2 compares two MLL steady-state operations with equivalent repetition rate (f_{rep} = 7.81 GHz $\leftrightarrow$ 8th harmonic), but obtained for two different PDL settings (with yet equivalent minimal delay τ). We observe that higher intra-cavity power (Fig.2b) and significant spectral broadening (Fig.2a) can be reached when the number of PDL pulse splitting increase. In both cases, the oscillation stability is maintained, and even enhanced for increased pulse splitting (blue lines in Fig. 2) due to the presence of a stronger MLL attractor, as attested by a steady-state reached sooner when the PDL spread efficiently the optical power over the fundamental period.

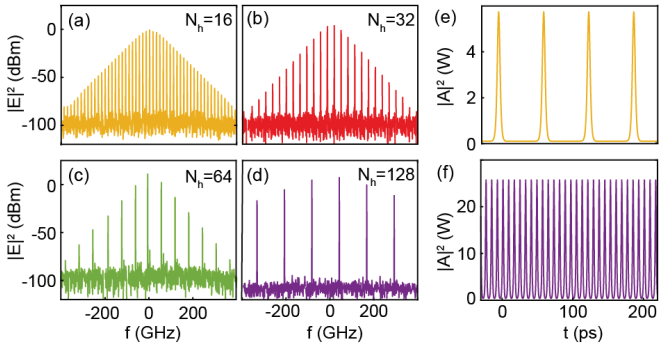

Fig. 4. Optical spectra obtained from the simulation parameters in Table.S1, for stable LCS excitation at different harmonics (N_h) of the MLL. Corresponding temporal intensity of the LCS Kerr comb for (e) N_h = 16 and (f) N_h = 128.

The maximal harmonic order achievable for such MLL, depends on the duty cycle of the pulse train generated, that is, the ratio between the pulse width and the pulse repetition rate: τ_p/T_{rep}. For Kerr comb MLL, the pulse width is fixed by the auxiliary cavity chromatic dispersion and the peak power of each individual pulse [15]. Conversely, the MLL repetition rate T_{rep} is determined by the PDL splitting ratio. To ensure solitons formation, the duty cycle needs to be small enough to avoid important soliton tails overlapping. In the latter case,

only type II Kerr combs appear to be achievable [16], and thus constitutes a limitation to the maximal achievable harmonic order of the soliton mode-locked cavity. To illustrate these dynamics, we performed a set of simulations considering the programmable nested cavity configuration of Fig. 1, including a Fabry-Pérot Resonator with an FSR of 976 MHz (i.e. $T_0 = 1024$ ps) and a main cavity parametrized as detailed in Supplement 1. The PDL modeled features delays encoded over a byte, i.e. $N = 8$ delay-lines, where each delay is related to the next by the recurrent relationship $\tau_{n+1} = \tau_n/2$, with a unitary delay $\tau_0 = 4$ ps. As a result, each delay is given by $\tau_n = 2^n\tau_0$ and the maximal cumulative delay by $\tau_{max} = (2^N - 1)\tau_0 = 1020$ ps. In total, 256 different MLL configurations can be selected for a single cavity, by changing the set of voltage $\{V_n\}_{1\leq n\leq N+1}$ of the PDL. The 256 configurations can be sorted by harmonic order $N_h = 2^n$, with $n \in \{0, 1, 2, 3, 4, 5, 6, 7, 8\}$, thus ranging from $N_h = 1$ to $N_h = 256$. Each set of harmonic order is then differentiated by the pulse splitting operation imposed by the PDL, and thus the gain condition required to achieve mode-locking. Fig.3 first summarizes the steady-states obtained numerically considering the cases where a single pulse is split into a sequence of replicas by the PDL, delayed by $\tau = T_0/N_h$. The delay is varied in order to span all the harmonic orders between $N_h = 2^4 = 16$ and $N_h = 2^7 = 128$. The Kerr comb FSR is successfully multiplied from 976 MHz ($N_h = 1$) to 125 GHz ($N_h = 128$) with stable operations clearly attested from the formation of a soliton pulse train (Fig. 3).

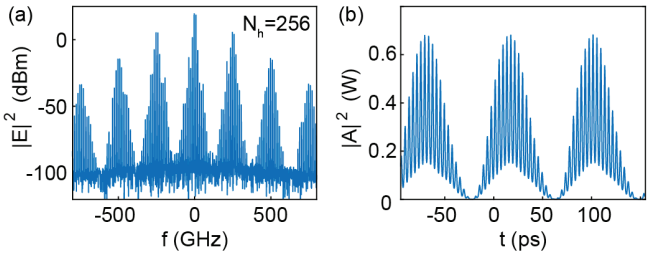

Fig. 5. Optical spectrum (a) and temporal intensity (b) of a type II Kerr comb obtained from the simulation parameters in Table.S1 for $N_h = 256$.

We however note that for $N_h = 2^8 = 256$, the MLL period becomes too close to the FPR intracavity pulse duration to ensure stable laser cavity soliton formation (i.e. $\tau_p/T_{rep}\sim1$); only Kerr comb of type II [16] could be obtained in this case illustrated in Fig.5. To some extent, this behavior may be mitigated by a suitable dispersion management of both cavities (in respect to the filter bandwidth), but however illustrate the limited pulse repetition rate tunability experimentally achievable for such an architecture.

In summary, we proposed a programmable fiber mode-locked laser based on a nested cavity configuration for flexible and reconfigurable Kerr comb generation. We numerically study and show that a programmable delay line, included in the main fiber cavity, can be leveraged for adjustable temporal pulse interleaving operation, so that to select a desired harmonic oscillation in the cavity. Specifically, we carefully considered the impact of the MZI carrier phase steps of the PDL on the modal selection efficiency and the locking bandwidth of the overall MLL architecture. Furthermore, we showed that the intrinsic PDL propagation loss imposes the gain and phase condition required for the lasing oscillation to be realized over 2^n round trips, so that to follow a rational mode-locking regime. In such a case, we reported that rational mode-locking mechanisms can lead to MLL harmonic oscillations when reaching a steady-state. Considering realistic experimental parameters for an integrated PDL [9] and fiber resonator [13], both nested in the main fiber cavity, we thus demonstrated stable passively mode-locked operation for the emission of tunable laser cavity solitons [4]. Besides reporting a proof of concept for LCS emission management in a flexible and reconfigurable way, we numerically demonstrate the potential of such an MLL architecture for the generation of reconfigurable Kerr combs over the whole GHz range, potentially up to the THz.

Funding. Horizon 2020 European Research Council (950618); Agence Nationale de la Recherche (ANR-10-LABX-48-01, ANR-20-CE30-0004); Conseil Régional Aquitaine (SPINAL).

Acknowledgement. This work received funding the European Research Council (ERC) under the European Union's Horizon 2020 research and innovation programme under grant agreement No. 950618 (STREAMLINE). B.W. acknowledges the support of the French ANR through the LabEx FIRST-TF and the Région Nouvelle Aquitaine (SPINAL).

Disclosures. The authors declare no conflicts of interest.

Data availability. Data underlying the results presented in this paper are not publicly available at this time but may be obtained from the authors upon reasonable request.

Supplemental document. See Supplement 1 for supporting content.

REFERENCES

1. D.J. Jones, S.A. Diddams, J.K. Ranha, *et al.*, Science, **288**, 635-639 (2000).
2. R. Paschotta, R. Häring, A. Garnache, *et al.*, Appl. Phys. B **75**, 445-451 (2002).
3. A. Laurain, D. Marah, R. Rockmore, *et al.*, Optica **3**, 781-784 (2016)
4. H. Bao, A. Cooper, M. Rowley, *et al.*, Nat. Photonics **13**, 384-389 (2019).
5. K. Minoshima, H. Matsumoto, Appl. Opt. **39**, 5512-5517 (2000).
6. F. Keilmann, C. Gohle, R. Holzwarth, Opt. Lett. **29**, 1542-1554 (2004).
7. D.J. Moss, R. Morandotti, A.L. Gaeta, *et al.*, Nature Photon. **7**, 597-607 (2013).
8. Y. Park, M.H. Asghari, T.-J. Ahn, *et al.*, Opt. Express **15**, 9584-9599 (2007).
9. B. Wetzel, M. Kues, P. Rotocki, *et al.*, Nat. Commun **9**, 4884 (2018).
10. H. Yu, S. Sciara, M. Chemnitz, *et al.*, Nat Commun **16**, 171 (2025).
11. L. Zhou, X. Wang, L. Lu, *et al.*, Chin. Opt. Lett. **16**, 101301- (2018).
12. M.C. Lo, R. Guzman, C. Gordon, *et al.*, Opt. Lett. **42**, 1532 (2017).
13. T. Bunel, M. Conforti, Z. Ziani, *et al.*, Opt. Lett. **48**, 275 (2023).
14. L.A. Lugiato, F. Prati, M.L. Gorodetsky, *et al.*, Phil. Trans. R. Soc. A. **376**, 20180113 (2018).
15. T. Herr, J.D. Jost, C.Y. Wang, *et al.*, Nature Photon. **8**, 145-152 (2014).
16. H. Bao, A. Cooper, S.T. Chu, *et al.*, Photon. Res. **6**, B67-B73 (2018).

REFERENCES

1. D.J. Jones, S.A. Diddams, J.K. Ranha, *et al.*, "Carrier-Envelope Phase Control of Femtosecond Mode-Locked Lasers and Direct Optical Frequency Synthesis", Science, **288**, 635-639 (2000).
2. R. Paschotta, R. Häring, A. Garnache, *et al.*, "Soliton-like pulse-shaping mechanism in passively mode-locked surface-emitting semiconductor lasers", Appl. Phys. B **75**, 445-451 (2002).
3. H. Bao, A. Cooper, M. Rowley, *et al.*, "Colliding pulse mode locking of vertical-external-cavity surface-emitting laser", Optica **3**, 781-784 (2016)
4. H. Bao, A. Cooper, M. Rowley, *et al.*, "Laser cavity-soliton microcombs", Nat. Photonics **13**, 384-389 (2019).
5. K. Minoshima, H. Matsumoto, "High-accuracy measurement of 240-m distance in an optical tunnel by use of a compact femtosecond laser", Appl. Opt. **39**, 5512-5517 (2000).
6. F. Keilmann, C. Gohle, R. Holzwarth, "Time-domain mid-infrared frequency-comb spectrometer", Opt. Lett. **29**, 1542-1554 (2004).
7. D.J. Moss, R. Morandotti, A.L. Gaeta, M. Lipson, "New CMOS-compatible platforms based on silicon nitride and Hydex for nonlinear optics", Nature Photon. **7**, 597-607 (2013).
8. Y. Park, M. H. Asghari, T.-J. Ahn, *et al.*, "Transform-limited picosecond pulse shaping based on temporal coherence synthesization", Opt. Express **15**, 9584-9599 (2007).
9. B. Wetzel, M. Kues, P. Rotocki, *et al*. "Customizing Supercontinuum generation via on-chip adaptive temporal pulse-splitting", Nat. Commun. **9**, 4884 (2018).
10. H. Yu, S. Sciara, M. Chemnitz, *et al.* "Quantum key distribution implemented with d-level time-bin entangled photons", Nat. Commun. **16**, 171 (2025).
11. L. Zhou, X. Wang, L. Lu, *et al.*, "Integrated optical delay lines: a review and perspective [Invited]", Chin. Opt. Lett. **16**, 101301 (2018).
12. M.C. Lo, R. Guzman, C. Gordon, *et al.*, "Mode-locked laser with pulse interleavers in a monolithic photonic integrated circuit for millimeter wave and terahertz carrier generation", Opt. Lett. **42**, 1532 (2017).
13. T. Bunel, M. Conforti, Z. Ziani, *et al.*, "Observation of modulation instability Kerr frequency combs in a fiber Fabry-Pérot resonator", Opt. Lett., **48**, 275 (2023).
14. L.A. Lugiato, F. Prati, M.L. Gorodetsky, *et al.*, "From the Lugiato-Lefever equation to microresonator-based soliton Kerr frequency combs", Phil. Trans. R. Soc. A. **376**, 20180113 (2018).
15. T. Herr, J.D. Jost, C.Y. Wang, *et al.*, "Temporal solitons in optical microresonators", Nature Photon. **8**, 145-152 (2014).
16. H. Bao, A. Cooper, S.T. Chu, *et al.*, "Type-II micro-comb generation in a filter-driven four wave mixing laser", Photon. Res. **6**, B67-B73 (2018)